Modeling of hydrogen isotope exchange from porous graphite

*A. Rai[a], R. Schneider [b], A. Mutzke [a], and M. Ravikant [c]

[a] *Max-Planck-Institute of Plasmaphysics, EURATOM Association, D-17491 Greifswald, Germany*

[b] *Institute of Physics, Ernst-Moritz-Arndt-University Greifswald, Felix-Hausdorff-Str.6, D-17489 Greifswald, Germany*

[c] *Department of Metallurgical and Materials Engineering, IIT Kharagpur, Kharagpur, West Bengal, India–721302*

Modeling of hydrogen isotope exchange from porous graphite

*A. Rai[a], R. Schneider [b], A. Mutzke [a], and M. Ravikant [c]

[a] *Max-Planck-Institute of Plasmaphysics, EURATOM Association, D-17491 Greifswald, Germany*

[b] *Institute of Physics, Ernst-Moritz-Arndt-University Greifswald, Felix-Hausdorff-Str.6, D-17489 Greifswald, Germany*

[c] *Department of Metallurgical and Materials Engineering, IIT Kharagpur, Kharagpur, West Bengal, India–721302*

Abstract: A 3D Kinetic Monte Carlo (KMC) model has been used to study the hydrogen isotope exchange from porous graphite at a single granule length scale (micrometers). The present KMC model is part of a previously reported multi–scale model developed by the authors [1]. SDTrimSP [2,3] simulations have been carried out and the results have been used to get some of the input parameters for the KMC where the diffusive–reactive aspect of H and D are studied. These SDTrimSP calculations show that the incident energetic ion beams lead to the development of inter–connected pores in the graphite sample. In the presence of these connected pores hydrogen molecule formation is not a local process. It takes place throughout the implantation zone and not only at the end of the ion range. For samples having less internal porosity mixing is very low. Therefore the internal structure of graphite, which affects the diffusion coefficient [4–7] and consequently molecule formation and atomic re–emission [8,9], plays the most crucial role for the H,D mixing. A new mechanism based on the KMC and SDTrimSP simulation is proposed to explain the experimental data.

* *Corresponding author:* Abha Rai (Abha.Rai@ipp.mpg.de)

Corresponding author address: Max-Planck-Institute of Plasmaphysics, EURATOM Association, Wendelsteinstrasse 1, D-17491 Greifswald, Germany.

keywords: Carbon, Diffusion, Hydrogen, Monte–Carlo modeling

PACS codes: 52.65.Pp

1 Introduction

In fusion machines hydrogen isotopes, deuterium and tritium, are used as fuel and graphite is used as a plasma facing material (PFM). Therefore, it is important to understand the transport and reactions of hydrogen isotopes in graphite. The graphites used as PFM in fusion devices are porous and consist of granules (few microns in size) separated by voids (fraction of a micron in size). These granules further consist of randomly oriented crystallites (a few nanometer in size) separated by micro–voids (fraction of nanometer in size) [10,11]. Diffusion plays a very prominent role here and due to its strong temperature dependence (the temperatures of the samples can vary between 300 K–2000 K), the time scales to be considered spans from pico–seconds to seconds. Therefore, the physics of the interaction of hydrogen with graphite used in the fusion devices is multi–scale in space (Å to cm) and time (picoseconds to seconds). For this reason a multi–scale model has been developed [1] . The model is a hierarchical multi–scale model, wherein simulations at the lower scales or experimental results wherever available are used as inputs to the simulations at higher scales. In other words, the idea is to use the insights gained from the microscopic (up to nanometers) models (MD or ab–initio methods) for modeling the transport at the meso–scale (up to micrometers) and further at the macro–scale (up to cms) in order to understand the physical processes contributing to macroscopic transport [4–7]. Fig. 1 explains the basic idea behind the 3D multi–scale model schematically and gives an example of the different computational tools used at various levels with the corresponding spatial and temporal scales. It will be shown later that for studying the hydrogen isotope exchange reaction simulations using the KMC (3D model at meso–scale) is sufficient. In the present work tools like classical molecular dynamics (HC Parcas) and binary collision cascade (SDTrimSP), have been used mainly to get the input parameters for the KMC model which is used to carry out all the reactive-diffusive processes (for details see sec. 3).

The results of hydrogen isotope exchange reaction are presented for the simultaneous bombardment of the hydrogen isotopes. Two important aspects of studying isotope exchange

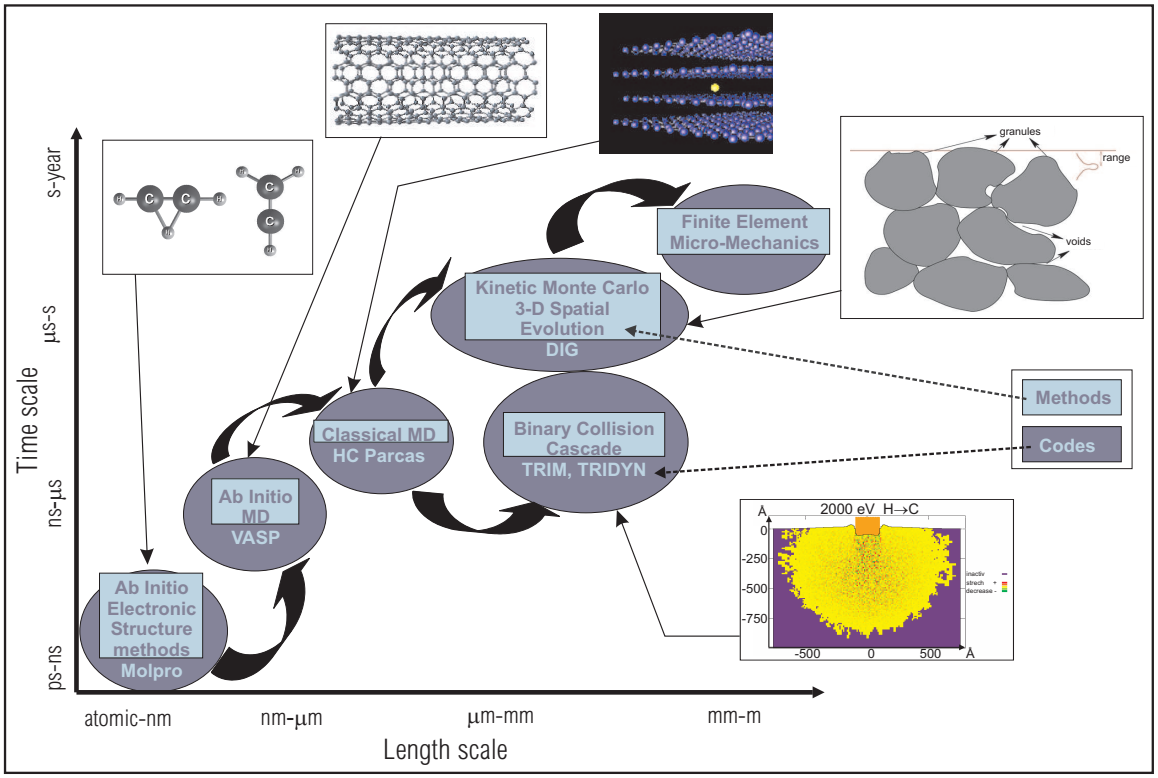

Fig. 1. Multi–scale schematic showing various methods and computational tools used at different spatial and temporal scales.

reaction are:

- To understand whether the hydrogen molecule formation takes place at the end of the incident ion range or it is happening throughout the implantation region.
- To understand whether the migration of hydrogen takes place in atomic or in molecular form.

If the molecule formation takes place throughout the implantation range then the isotope exchange reaction can be used as a cleaning (retrieving the retained tritium from the sample) method of a graphite target material saturated with tritium by bombarding it with deuterium or hydrogen.

2 Experimental observations by Chiu *et al.*

In the present work the simulation results are compared to experimental results reported by Chiu *et al.* [12,13] where a graphite target was bombarded with ion beams of H^+ or D^+ (or both H^+ and D^+ simultaneously) and the effect of different hydrogen isotopes on processes like molecule formation or trapping were studied. In the first experimental campaign [12] crystalline graphite samples were bombarded simultaneously with H^+ and D^+ ion beams having:

- completely overlapping ion energy ranges (10 keV H^+ and 9.4 keV D^+),
- completely separated ion energy ranges (10 keV H^+ and 700 eV D^+),

and the re–emission time traces were measured.

They observed that in steady–state the re–emitted signal is independent of the energy range separation of two ion distributions. This gives an indication that the hydrogen diffusion takes place in atomic form too and the molecule formation does not take place locally at the end of the ion range. However, it was also pointed out that H–D mixing is a function of crystal structure and damage. In the absence of incoming energetic ions, the samples which are 'virgin' (having very less damage), molecules are indeed formed locally at the end of the ion range. Structural dependence of re–emission was also observed by the present authors in previous simulations [9].

In the follow–up experiments [13] TDS (thermal desorption spectroscopy) was used to study the thermal release from an HPG99 sample simultaneously implanted by H^+ and D^+ to a fluence of $\sim 5 \times 10^{20}$ H^+ or D^+/m^2 (below saturation fluence for energy > 1 keV). HD mixing was studied for various energy separations and it was found that HD formation was a very sensitive function of $D^+ - H^+$ range separation. This is in agreement with the observations made by Möller and Scherzer's [14] for sequential implantation but in contrast to the previous experiment by Chiu [12]. Now onwards these two experimental

scenarios will be referred as TDS and SSR (steady–state re–emission) by Chiu.

In the present work a porous graphite structure [8,15] is created and the effect of hydrogen isotope mixing during the simultaneous bombardment of H and D ion beams having overlapping and non–overlapping profiles is studied.

3 Description of the 3D KMC model

A 3D multi–scale model has been developed to model the hydrogen isotope reactive–diffusive transport in porous graphite [8,9]. The two–region model developed by Haasz *et al.* [10] has been implemented distinguishing the atomic and molecular transport processes within the bulk and surface region on the graphite crystallites. Hydrogen atoms and molecules within the crystallites and on the bulk–void interface are treated as different species and have different transport behavior due to the fact that they experience different chemical surroundings. In the present work we simulate the physics at meso–scales where a $100\,nm \times 100\,nm \times 300\,nm$ sized granule of graphite is taken and Kinetic Monte–Carlo (KMC) is used. In KMC scheme all the thermally activated processes taking place in the system are parametrized in terms of the jump attempt frequency ω_o^j, the migration energy E_m^j, and the jump distance L_j [4–7]. The jump distance L_j corresponds to the distance jumped by an atom or molecule in a specified direction after overcoming the j^{th} energy barrier with migration energy E_m^j.

Within the KMC ansatz, all attractive potentials are considered as traps, by either covalent bonding or adsorption. Therefore, the term trap is loosely used for even adsorption events. The energy for an atom to (i) detrap, (ii) dissociate or (iii) desorb is referred to as the migration energy. This is because any of these events leads to a migration of the trapped atom. The present model simulates the reactive–diffusive transport of the thermalized hydrogen in graphite. The collisional cascade effects are taken into account by using a depth distribution corresponding to the range of the incident ions as calculated with SDTrimSP.

As explained earlier, for setting up the 3D KMC simulation various input parameters are needed and in this section the method/justification of using them are explained.

3.1 internal structure

In the experiment of Chiu *et al.*[12] the graphite sample had a density of 1.84 g/cm^3 and the grains were composed of crystallites of the order of 10-100 nm. No direct experiment was performed to calculate the internal structure of the sample, namely, void size and void fraction. One can get a rough estimate by comparing the given density of the sample with the density of the standard graphite sample (2.2 g/cm^3) and this leads to void fraction of $\sim 20\%$ for the sample used in the experiment. In KMC simulation a graphite sample with dimension of $100\,nm \times 100\,nm \times 300\,nm$, in the x,y and z-direction with cubical voids of size $50\,nm$ was constructed. The sample had the void fraction of 20 %. The basic cell size used to construct the above geometry was $0.5\,nm$ and which is small enough to accommodate the smallest jump length scale present in the system. Since for the problem we intend to address, the spatial scale is $\sim 300\,nm$ the simulations are performed at the meso–scales only (using 3D KMC).

Using the above internal structure KMC simulation was performed to study the hydrogen isotope mixing at sample temperature of 600 K, H and D ion beams with flux of $3 \times 10^{18}\,atoms/m^2\,s$ and energies of $1\,keV$ and $6\,keV$, respectively. For the completely overlapping profiles of the H and D ion beams ideal mixing was observed ($H_2 : HD : D_2$ ratio of the released molecules was 1:2:1). Whereas, in the case of the completely separated ion profiles hydrogen isotope mixing was not as pronounced as reported in the experiments where for SSR experiment by Chiu, HD/D_2 ratio of 1.4 (till $D^+ - H^+$ energy separation of $10\,keV$) and for TDS experiment, HD/D_2 ratio of ~ 0.25 (till $D^+ - H^+$ energy separation of $8\,keV$) was observed. A scan using KMC over the different internal structure configurations, *e. g.*, void fraction and void size was done. At low sample tem-

peratures the mixing of the two hydrogen isotopes was still very small. Fig. 2 shows the time development of the released HD/D_2 ratio at 1200 K. It can be seen that after the initial transient phase the HD mixing increases with time because the implanted D-atom distribution gradually builds up towards the surface once the local saturation is reached.

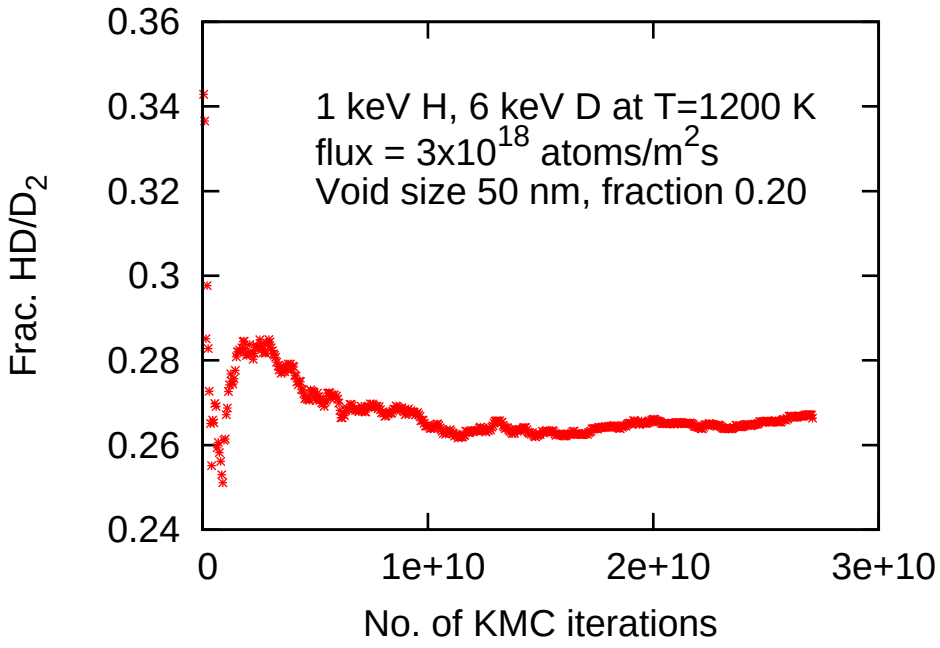

Fig. 2. Fraction of the released HD/D_2 as a function of the no. of KMC iterations. The sample was at 1200 K temperature with 20% void fraction and it was bombarded with H and D ion beams with flux of $3 \times 10^{18}\, atoms/m^2\, s$ and energies of $1\, keV$ and $6\, keV$, respectively.

In fig. 3 the dependence of HD mixing on $D^+ - H^+$ energy separation is presented. The simulation result follow the similar trend like experiment (TDS by Chiu) for an unsaturated sample. The HD/D_2 ratio in both the cases is ~ 0.25 for $D^+ - H^+$ energy separation $> 2keV$. For the saturation to set in during simulations, a very long run time is needed and therefore the comparison is made only with the unsaturated sample case. So it is observed that in experiments both TDS and SSI mixing is observed at the room temperature whereas in KMC simulations it is observed only at higher temperatures (> 1200 K). As will be seen later, uncertainty about the exact internal structure *e.g.* void fraction, size distribution and orientation, alone is not enough to explain this discrepancy. One of the major goal of the present work is to understand this discrepancy.

This observation is in agreement with TDS experiment but in contrast with SSR experi-

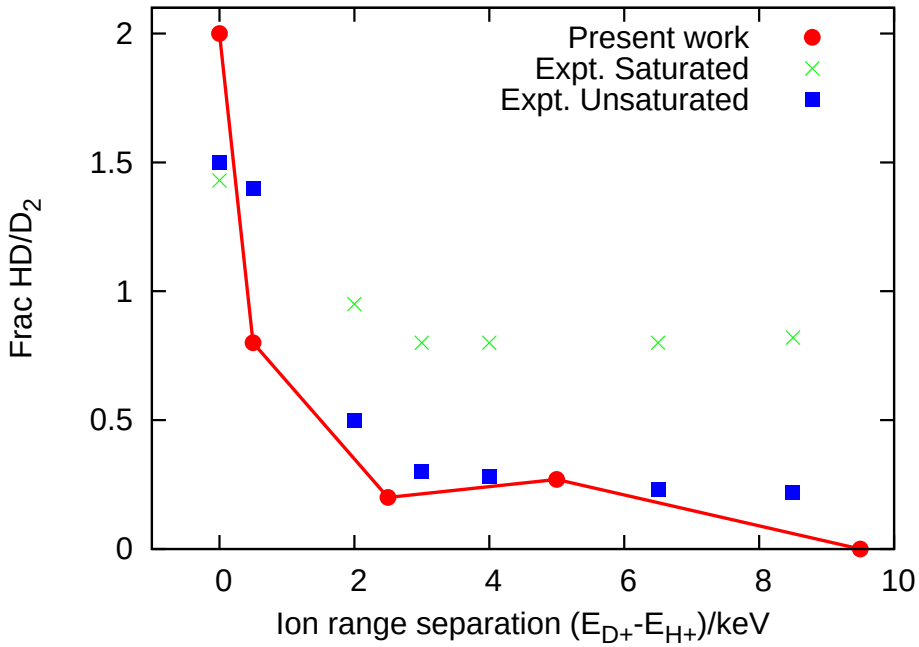

Fig. 3. Fraction of the released HD/D_2 as a function of $D^+ - H^+$ energy separation. The simulation result is compared to TDS experimental data by Chiu [13]. The sample used in the simulation was at 1200 K temperature with 20% void fraction and it was bombarded with H and D ion beams with flux of $3 \times 10^{18}\, atoms/m^2\, s$ and energies of $1\, keV$ and $6\, keV$, respectively.

ment by Chiu where mixing is practically independent of the $D^+ - H^+$ energy separation. It was speculated that the effect of fluence of the incident ion beams on the penetration depth might have contributed to this discrepancy. Using SDTrimSP simulations it was found that the fluence of the ion beam has a negligible effect on the penetration depth of the two hydrogen isotopes. SDTrimSP simulations were performed to calculate the damage caused by the incident ion beams. Fig. 4 shows the density change of a graphite sample having initial density of 1.84 g/cm^3 due to the bombardment of H and D ions beams having different energy combinations. The simulation was done with H:D as 1:1 and the fluence of 10^{20} H or D $/cm^2$. One can estimate the damage and the change in the void fraction caused by the energetic ion beams. From these calculations one sees that the void fraction of the sample should be around 60 % instead of 20 % as was estimated on the bases of the density of the sample used in experiment. We have earlier also reported that the internal structure of the graphite plays a crucial role in the dynamics of the molecule formation and release process [8]. Now onwards all the KMC simulation results presented will have void fraction of 60 %. Here one can see that SDTrimSP simulations were used

in a feedback kind of mode where SDTrimSP method gave a good physical insight at the damage created in the sample and then this was used to rectify the internal structure input used in KMC.

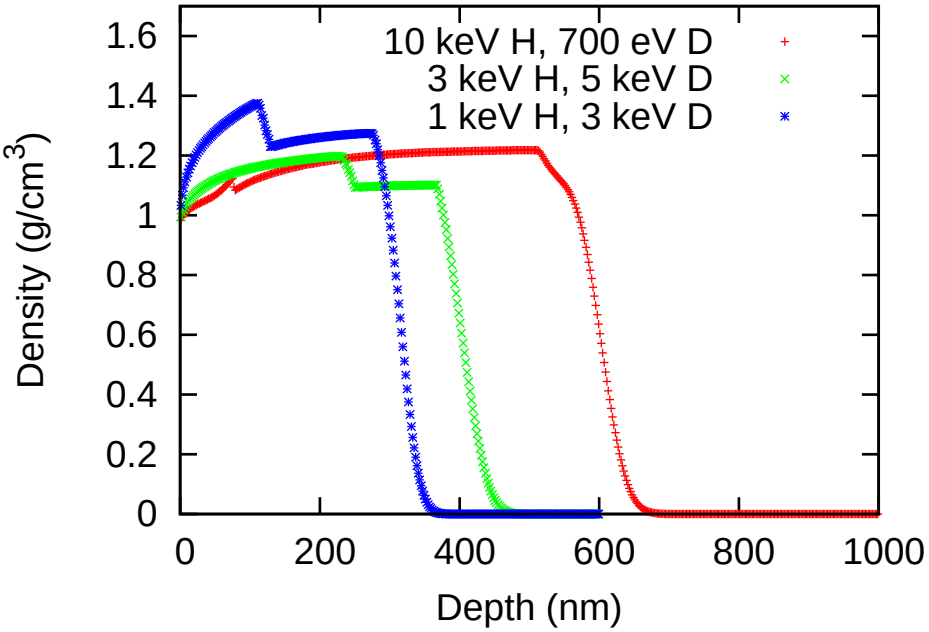

Fig. 4. Density change profile calculated using SDTrimSP for different incident ion energies combination.

3.2 profiles of the incoming ion beams

The sample was bombarded with the H and D ion beams with energy of 1 keV and 6 keV, respectively. SDTrimSP was used to find the effect of the incoming H and D ion beams *e.g.* penetration depth or profile of the thermalized ions beams after the collisional cascade in the sample. The profiles of the thermalized H and D ions in the sample were approximated with a Gaussian, this corresponds to the mean penetration depth of 25 nm and 135 nm with standard deviation of 15 nm and 30 nm for 1 keV and 6 keV ion beams, respectively.

3.3 trapping probability

SDTrimSP was used to find the damage caused by the incident ion beams and using this the trapping probability of the sample was calculated. A scan over the trapping probability was done ranging from 10^{-4}–0.2 and it was found that the mixing has a very weak dependence on the trapping probability. In the present case the trapping probability was taken as 0.0003 in KMC. In highly porous structures like the one collected from the leading edge of the neutralizer from Tore–Supra, it can be high, of the order of 0.007 [16].

3.4 diffusive processes parameters(ω_o^j,E_m^j, L_j)

The input parameters to describe diffusive processes (ω_o^j,E_m^j, L_j) have been taken from molecular dynamics simulations and experiments. The following processes have been included into the model for a hydrogen atom

- Diffusion within the crystallites: short ($0.015\ eV$, $0.38\ nm$, $6.8{\cdot}10^{12}\ s^{-1}$) or long ($0.269\ eV$, $1.0\ nm$, $2.74 \cdot 10^{13}\ s^{-1}$) jumps [8]
- Surface diffusion ($0.9\ eV, 3.46\ nm, 1.0 \cdot 10^{13}\ s^{-1}$) [17,18]
- Trapping (based on predefined trap site distribution or trapping probability)
- Detrapping ($2.6\ eV, 0.3\ nm, 1.0 \cdot 10^{13}\ s^{-1}$) [18]
- Going into the bulk ($2.67\ eV, 0.3\ nm, 1.0 \cdot 10^{13}\ s^{-1}$) [19]
- Desorption ($1.91\ eV, 0.2\ nm, 1.0 \cdot 10^{13}\ s^{-1}$) [20]
- Recombination (Not a thermally activated process. Treated using Smoluchowski boundary condition [8,21]).

Similarly a hydrogen molecule can undergo the following processes

- Diffusion ($0.06\ eV, 0.2\ nm, 1.0 \cdot 10^{13}\ s^{-1}$)
- Dissociation ($4.48\ eV, 0.2\ nm, 1.0 \cdot 10^{13}\ s^{-1}$)
- Desorption (H_2 is chemically inactive species, so it gets desorbed as soon as it reaches the geometrical surface)

- Detrapping (detrapping of two trapped hydrogen atoms close enough to form molecule): (2.3 eV, 0.4 nm, $1.0 \cdot 10^{13}$ s^{-1}) [22].

Finally, the parameters like trapping probability and the profiles of the incoming ion beams obtained from SDTrimSP simulations were used as inputs in the 3D KMC model. As explained previously, the physics aspects of the micro–scale are not included explicitly here. They are included only through the use of various parametrized quantities (like energy barriers and jump lengths for various processes calculated using MD) obtained from micro–scale simulations as input parameters (in line with the multi–scale modeling).

4 Results

Fig. 5 shows the temperature dependence of the re–emitted HD and D_2 flux. It can be seen that the HD mixing level increases with temperature, although the dependence is rather weak. The reason behind this observation is discussed in the next paragraph on the basis of the profiles of various species in the sample. Simulation result follows the experimental trends reported by Franzen *et al.* (fig. 1 [23]) for EK98 graphite sample at elevated temperatures.

The KMC code developed in the present work is capable of giving better insight into the detailed dynamics of the various species. It is not possible to perform such detailed diagnostic in the experiment and thus, simulations help us to get an insight into the problem at hand. As an example, Fig. 6 shows the temperature dependence of various quantities that can be diagnosed with the code. Since the statistical errors are very small the error bars are not shown here. It has been observed that at lower temperatures all the hydrogen present in the system is trapped at the trapping sites and hydrogen is released mainly in the molecular form and as the temperature increases detrapping sets in and hydrogen is released in the atomic from. This is also in agreement with the experimental trends observed by Franzen (fig. 4 [23]) and previous simulations by the present authors ([8]) where a detailed comparison with the corresponding experimental data was done. It

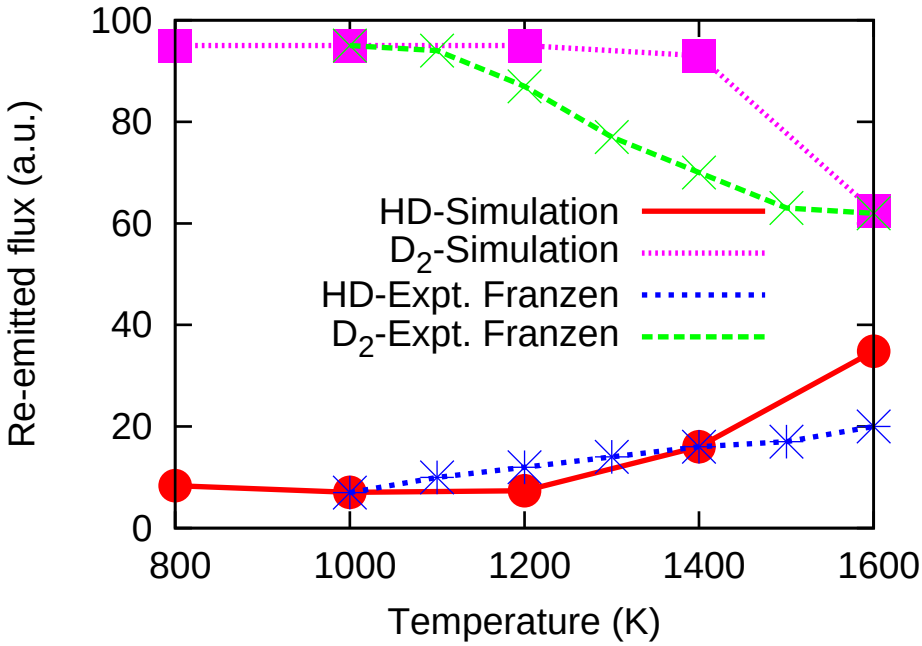

Fig. 5. Temperature dependence of re–emitted HD and D_2 flux obtained using KMC. The sample with 0.60 void fraction and void size 50 nm was simultaneously bombarded by 1 keV H and 6 keV D ion beams with flux of $3 \times 10^{18}\, atoms/m^2 s$. The results are compared with the experimental data by Franzen *et al.* [23] for EK98 graphite sample.

was shown that the re–emission and the temperature at which it starts is very sensitive to the internal structure, energy and the fluence of the incoming ion beam. Increase in the porosity delays the onset of hydrogen release in atomic form. From the energetic consideration, a graphite with void fraction of 15 % starts releasing H in atomic form around 1000 K, but due to the increased porosity even after getting detrapped locally they get trapped again in the course of out–diffusion. The temperature at which the trapping–detrapping processes is frequent enough that it leads to a quick diffusion of hydrogen in atomic form is termed here as the temperature where 'effective detrapping' process starts. We see here also clearly that since we have high porosity (60 % void fraction) the release of atomic H starts only around 1600 K (Fig. 6a). At lower temperature most of the H and D atoms are present in the trapped form (Fig. 6b) and around 1600 K the effective detrapping starts. Since H ions are distributed closer to the surface (1 keV energy) they can escape through the surface in molecular form (HD/H_2 ratio in Fig. 6c) whereas the D atoms which are distributed deeper, get trapped again and therefore the fraction of D-trapped atoms is much higher (Fig. 6b) leading to lesser release of D_2 than H_2 (Fig. 6c

and Fig. 6d).

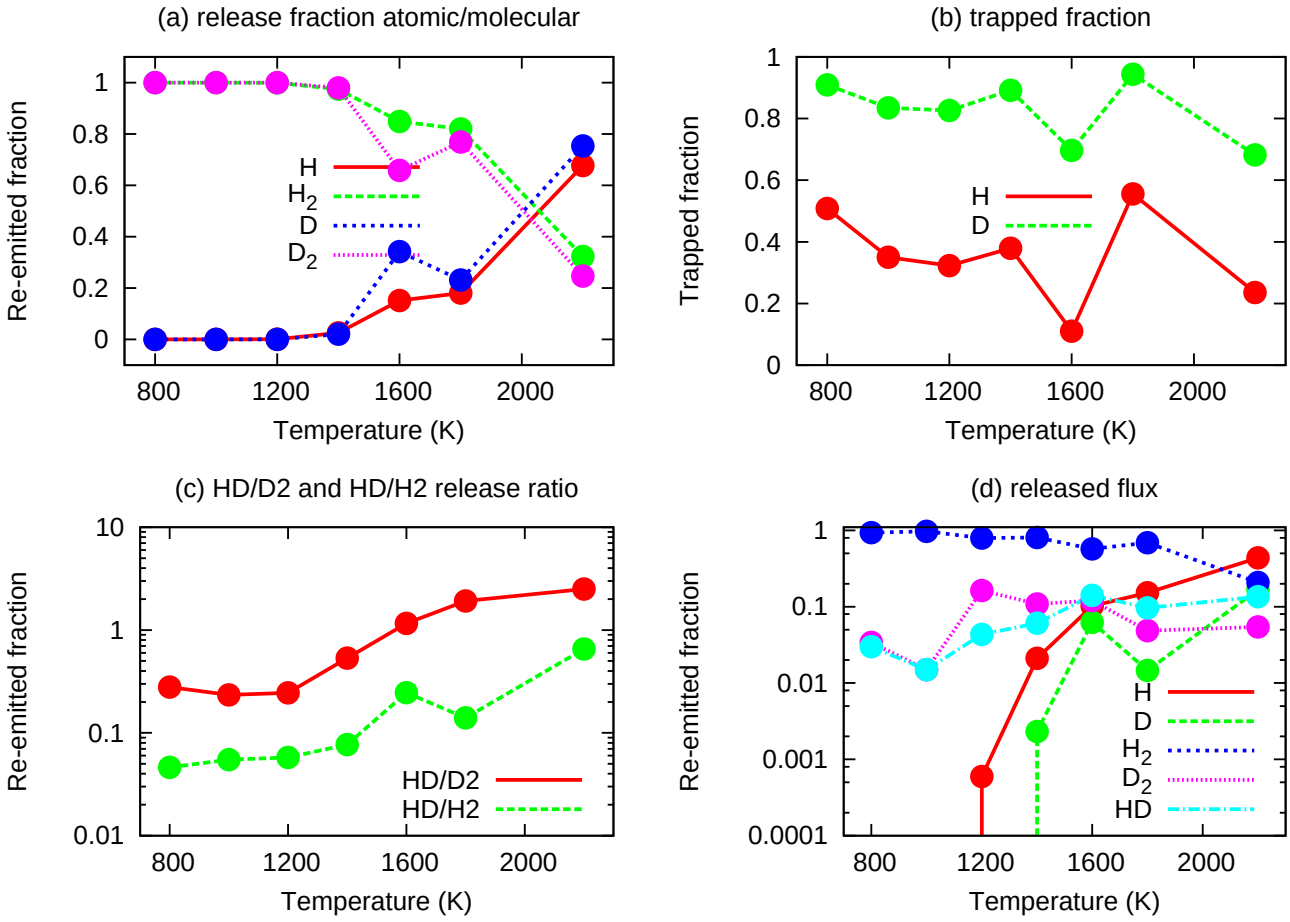

Fig. 6. Temperature dependence of the various observed quantities obtained using KMC. The sample with 0.60 void fraction and void size 50 nm was simultaneously bombarded by 1 keV H and 6 keV D ion beams with flux of $3 \times 10^{18}\, atoms/m^2 s$.

Once the threshold temperature where the 'effective detrapping' process starts is achieved, temperature of the sample has a weak dependence on the mixing process. A possible explanation to the onset of significant levels of mixing only at higher temperatures could be the effect of the enhanced diffusion due to the local heating or thermal spikes produced during the interaction of the energetic H^+/D^+ ion and the graphite target atoms. *'Collisional'* thermal spikes in a more general sense results from any cascade which finally thermalizes towards the temperature of the surrounding material.

Again, SDTrimSP was used to get morphology of the affected area due to collisional cascade caused by the incoming ion beam for a given energy and particle flux. Fig. 7

shows the SDTrimSP calculation of the morphology of penetrating H ion beams of 400 eV and 1 keV energies. Taking this into account we assume the evolution of a cascade around a linear ion track and affected area in the target to be a cylinder. A simplified model of a cylindrical thermal spike is now presented. The radius r (Fig. 7) and the height h of the cylinder (approximated by the penetration depth of the ion beam) is estimated using SDTrimSP. For 1 keV ion beam r and h are approximated by 30 nm and 50 nm respectively.

If E is the energy of a single H or D atom, then the total energy deposited per unit time by a source with flux of $\phi(= 3 \times 10^{18}\, atoms/m^2\, s)$ to a surface (assumed cylindrical here) of radius r will be $\phi\pi r^2 E$. The corresponding temperature rise (ΔT) per unit time can be calculated using the balance equation

$$\phi\pi r^2 E = \rho\pi r^2 hc\Delta T + Q. \tag{1}$$

Neglecting energy loss due to heat transfer Q, the system is translationally invariant in the direction of the depth x. For 1 keV ion beam this equation indicates that the temperature rise due to a thermal spike can be above $10^4\, K$. It should be noted that this high temperature rise is a very local phenomenon and is not the temperature of the sample. This high value of temperature is correct only in the close vicinity of the ion track and as will be shown next, it decays down to the ambient temperature within pico–seconds. Temperature is a global parameter of a sample and it is the characteristics of a thermalized system. In the present analysis it is used only to derive the profile and the decay time of the heat spike and the calculation of enhanced diffusion as a consequence of this. When a temperature is specified for the KMC simulation it is implied as the uniform temperature of the sample.

Now a more detailed analysis is presented to estimate the lifetime and the temperature rise due to a thermal spike. For simplicity, a zero temperature of the material is assumed as initial condition. At t=0, the time of ion incidence, energy E is deposited within a negligible time interval along the ion track. The energy deposition function idealised by a

planar δ function in circular symmetry leads to the initial temperature profile along the track of the ion as

$$|\frac{dE}{dx}|\delta(\bar{r}) = \rho\, c\, T(r, t = 0) \tag{2}$$

with the normalization $\int 2\pi r\delta(\bar{r})dr = 1$. Here c $(= 0.714\, J/gK)$ and ρ $(= 1.85\, g/cc)$ are the specific heat and mass density of the sample, respectively. Around the track, a thermal wave develops in radial direction according to the law of thermal diffusion

$$\frac{\partial T}{\partial t} = \frac{\lambda}{\rho c}\Delta T = \frac{\lambda}{\rho c}\frac{1}{r}\frac{\partial}{\partial r}(r\frac{\partial T}{\partial r}) \tag{3}$$

with λ as the thermal conductivity. The solution of this equation gives the radial profile of the temperature at a given instant of time

$$T(r, t) = |\frac{dE}{dx}|\frac{1}{4\pi\lambda t}exp(-\frac{\rho c r^2}{4\lambda t}). \tag{4}$$

In the limit of $\tau \to 0$, this solution fulfills eq. 2 as

$$\frac{1}{\pi\tau}e^{-\frac{-r^2}{\tau}} \to \delta(\bar{r}) \tag{5}$$

Using this solution one predicts close to the ion track temperatures of a few $10^4\, K$ and this thermal pulse dissipates quickly at larger distances from the track. Therefore, if a heat spike is formed, it can live for 1–100 ps until the spike temperature has cooled down essentially to the ambient temperature.

The value of the diffusion coefficient (D) of the hydrogen due to surface diffusion reported by experiments [17] and KMC simulations [4] is given by $1.2e^{\frac{-0.9}{k_B T}}\, cm^2/s$, here k_B is the Boltzmann constant. This implies that the surface diffusion coefficient at $10^4\, K$ is $\sim 10^3\, m^{-2}s^{-1}$. Using this value of D, the displacement (Δx) of a hydrogen atoms in time Δt will be $2D\Delta t$. The typical lifetime of a heat spike is $\sim 1 - 100 \times 10^{-12}\, s$. This leads to Δx in the range of $1 - 100\, nm$. Depending on this simple estimate one can conclude that even if the sample is bombarded with two ion beams of non–overlapping profiles, the

enhanced diffusivity due to the thermal spike gives rise to a very dynamic system and leads to the considerable amount of mixing. Since other processes like trapping–detrapping etc. are also present which hinders the free movement of atoms and therefore complete mixing, one does not observe ideal mixing. In the present simulations the phenomenon of enhanced diffusion due to the heat spike is implemented by increasing the temperature of the sample uniformly. The simple estimate presented above, gives a possible argument of the observation that mixing appears only at higher temperatures in KMC simulations as opposed to the experiments where mixing was observed at room temperature.

Fig. 8 shows the void fraction dependence of the H–D mixing for a graphite sample having void size $50\,nm \times 50\,nm \times 5\,nm$ at 1800 K. It is clearly seen that for the void fraction $\sim$ 60 % there is good mixing of the H–D atoms leading to the ratio of HD/D_2 around 2.0. This choice of void fraction is also in agreement with the SDTrimSP estimates. From this result it is clear that the identification of the higher void fraction and the process of enhanced diffusion due to the thermal spike were the most crucial factors contributing to the occurrence of the mixing at high temperature ($\sim$ 1600 K) in the simulations compared to the experiments (at 300 K).

To recapitulate, SDTrimSP simulations show that porous structures are indeed created due to the damage caused by the incoming ion beams and at room temperature the local heating due to the incoming ion beams lead to the enhanced release and diffusion of the trapped H and D locally. When these results are used in the KMC model, the fact that the mixing of H and D takes place only if the two ion profiles are well connected through the internal porosity, is also observed. This explains clearly the experimental result where isotope mixing is observed at room temperature for completely separated ion beam profiles.

Fig. 9 shows the dependence of released HD/D_2 on the void size of the sample. The incident ion beam is bombarded along the z–direction and the x–y plane is normal to it. Following three configuration of the void size were taken

(1) case 1: $50\,nm \times 50\,nm \times 50\,nm$ void size

(2) case 2: $50\,nm \times 50\,nm \times 5\,nm$ void size

(3) case 3: $50\,nm \times 50\,nm \times 100\,nm$ void size

The error bars are very small and therefore they are not shown in the figure. It can be seen that for case 3 where we have elongated voids along the z–direction HD/D_2 is maximum. This is due to the fact that the elongated voids provide a quicker diffusion channel for the ion situated deeper into the sample and leading to the surface and eventually mixing with the ions distributed closer to the surface and thus better mixing. Actually, this is exactly the kind of geometrical internal structures found in the co–deposited layers of Tore-Supra where asparagus like structures are observed and one observes elongated voids.

5 Summary

The isotope exchange reaction of hydrogen in graphite was studied both for completely separated and completely overlapping ion profiles. The main factors affecting the mixed molecule formation are:

- internal structure of graphite, which affects diffusion coefficient and consequently molecule formation and atomic re–emission
- threshold temperature for the mixing, which again depends on the internal structure of the graphite.

A scan over the trapping probability up to a value of 0.2 shows that the isotope mixing has a weak dependence on the trapping probability of H and D atoms.

The mixed molecule formation during the exposure to H and D ions with completely separate ion profile (penetration depths) indicates that due to a thermal spike leading to the enhanced diffusivity and a very dynamic system, hydrogen molecule formation is not a local process. It takes place throughout the implantation zone and not only at the end of the ion range.

References

[1] A. Rai, M. Warrier, and R. Schneider. *Computational Materials Science*, 46:469–478, 2009.

[2] A. Mutzke and W. Eckstein. *Nucl. Instr. amd Meth. B*, 266:872–876, (2008).

[3] W. Eckstein A. Mutzke, R. Schneider and R. Dohmen. SDTrimSP: Version 5.00. *IPP, Report*, (12/8), 2011.

[4] M. Warrier. *Ph.D. Dissertation, Faculty of Mathematics and Natural Science, Uni. Greifswald, Germany*, (2004).

[5] M. Warrier and R. Schneider *et al. J. Nucl. Mater.*, 337-339:580–584, (2005).

[6] M. Warrier and R. Schneider *et al. Physica Scripta*, T108:85, (2004).

[7] M. Warrier and R. Schneider *et al. Contrib. Plasma Phys.*, 44(1-3):307–310, (2004).

[8] A. Rai, R. Schneider, and M. Warrier. *J. Nucl. Mater*, 374:304–312, (2008).

[9] R. Schneider and A. Rai *et al. J. Nucl. Mater.*, 367-370:1238–1242, (2007).

[10] A. A. Haasz *et al. J. Appl. Phys.*, 77(1):66–86, (1995).

[11] W. Möller. *J. Nucl. Mater.*, 162-164:138–150, (1989).

[12] S. Chiu and A. A. Haasz. *J. Nucl. Mater.*, 196-198:972–976, (1992).

[13] S. Chiu and A. A. Haasz. *J. Nucl. Mater.*, 210:34–42, (1994).

[14] W. Möller and B. M. U. Scherzer. *Appl. Phys. Lett.*, 50(26):1870–1872, (1987).

[15] M. Warrier and R. Schneider *et al. Nucl. Fusion*, 47:1656–1663, (2007).

[16] A. Rai and R. Schneider *et al. J. Nucl. Mater.*, 386-388:41, (2009).

[17] R. A. Causey *et al. J. Vac. Sci. Technol. A*, 4(3):1189–1192, (1986).

[18] K. L. Wilson *et al. Atomic and plasma-material interaction data for fusion (supplement to the journal Nuclear Fusion)*, 1:31–50, (1991).

[19] G. Federici and C. H. Wu. *J. Nucl. Mater.*, 186(2):131–152, (1991).

[20] K. Ashida *et al. J. Nucl. Mater.*, 128 & 129:792, (1984).

[21] M. V. Smoluchowski. *Z. Physik Chem.*, 107:463, (1957).

[22] H. Atsumi. *Phy. Scr.*, T103:77–80, (2003).

[23] P. Franzen and E. Vietzke *et al. J. Nucl. Mater.*, 196-198:967–971, (1992).

List of Figures

(a)

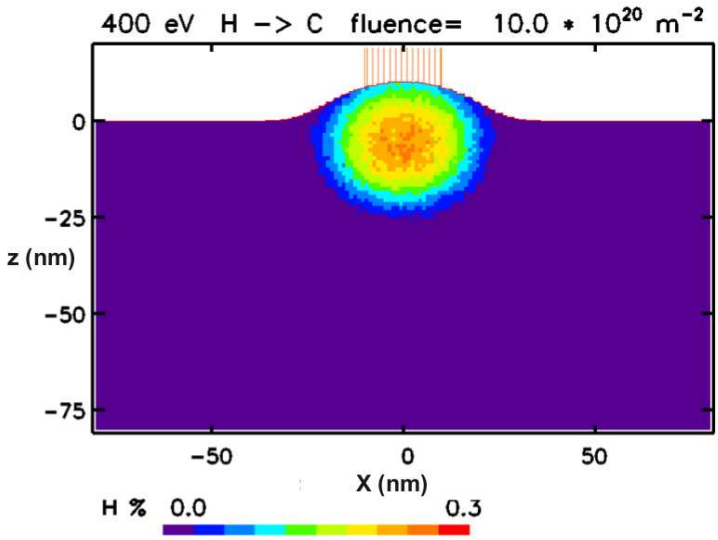

(b)

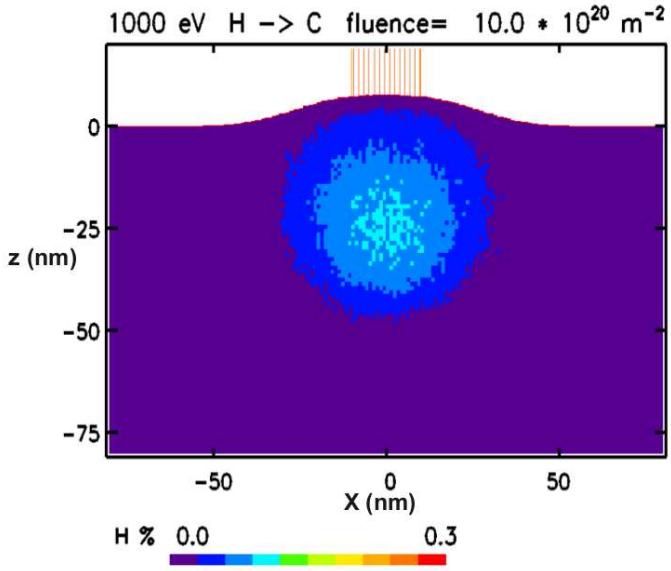

Fig. 7. SDTrimSP calculations showing the affected area of the target due to incoming ion beam having (a) 400 eV and (b) 1 keV energy.

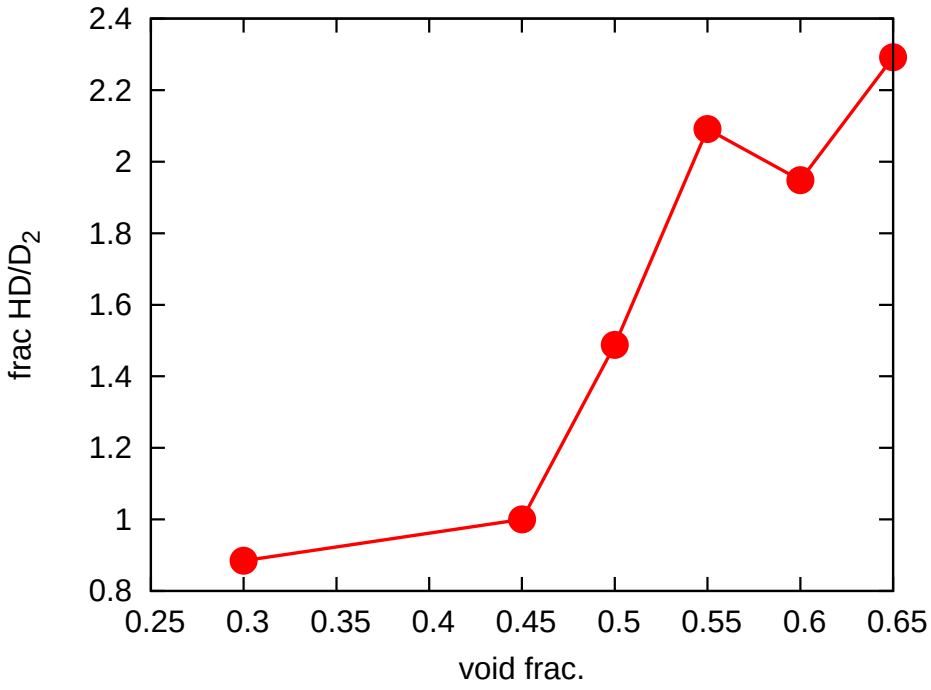

Fig. 8. Released HD/D_2 as a function of the void fraction of the sample (void size $50\,nm \times 50\,nm \times 5\,nm$) at 1800 K bombarded by H and D ion beams (flux $3 \times 10^{18}\,atoms/m^2 s$) with energy of 1 keV and 6 keV respectively.

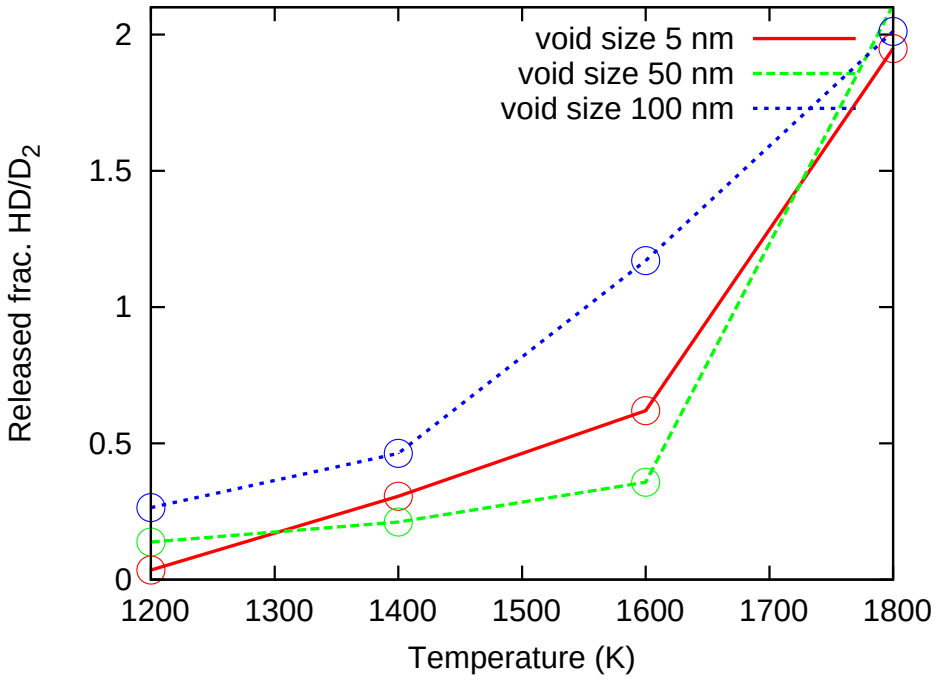

Fig. 9. Released HD/D_2 as a function of the void size of the sample (void fraction 60 %, 1800 K). The sample was bombarded by H and D ion beams (flux $3 \times 10^{18}\,atoms/m^2 s$) with energy of 1 keV and 6 keV respectively.